Supporting Information

Personalized demand-responsive biphasic microneedle patch for smart drug administration

Shuyue Deng,‡[a] Yao Shuai,‡[b] Shibo Zhang,[a] Caixia Sun,[a] Lei Chang,[c] Jie Xu,[b,d] Ling Tong,[b] Qunsheng Ji,[b] Min Li,[d] Jianjun Dai,*[a,e] Yanmin Ju*[a]

[a] College of Pharmacy, China Pharmaceutical University, Nanjing 211198, China

[b] Oncology and Immunology Unit, WuXi AppTec, Nantong 226000, China

[c] Department of Cellular and Molecular Medicine, University of California San Diego School of Medicine, La Jolla, CA, USA

[d] School of Computer Science and Engineering, Central South University, Changsha 410006, China

[e] MOE Joint International Research Laboratory of Animal Health and Food Safety, Key Laboratory of Animal Bacteriology, Ministry of Agriculture, College of Veterinary Medicine, Nanjing Agricultural University, Nanjing 210095, China

EXPERIMENTAL SECTION

Drug content. The drug content was determined by HPLC coupled to ultraviolet detection (HPLC-UV) analysis (LC-20A, Shimadzu, Japan). In brief, 2 mg NCs powders were weighed and dissolved in 7 mL acetonitrile, then 3 mL deionized water was added to fix the volume to 10 mL, shaken and filtered. HPLC-UV experimental conditions: reversed phase C18 column (250 mm by 4.6 mm; inner diameter, 5 μm particle size). Acetonitrile and distilled water (7:3 ratio, v/v) formed the mobile phase. The injection volume was 20 μL, with a flow temperature of 30°C and flow rate of 1 mL/min.

Drug release from LPF NCs in vitro. An appropriate amount of LPF NCs was put into a dialysis bag, clamped, and the bag was placed into a centrifuge tube with 100 mL PBS (pH=7.4) solution with 25% ethanol as release media. Centrifuge tubes containing dialysis bags were incubated in a constant temperature shaker at 37°C and shook at 200 rpm. A certain amount of release medium was taken at predetermined time intervals as sample solution (0, 1, 2, 3, 5, 6, 7, 8, 10, 12, 16, and 18 days) to be tested and replenished with the same volume of fresh release medium. The sample solution was extracted with DCM and the mobile phase was added. The DCM was evaporated and the LNG amount was assayed by HPLC-UV. HPLC-UV experimental conditions: reversed-phase C18 column (250 mm by 4.6 mm; inner diameter, 5 μm particle size). Acetonitrile and distilled water (7:3 ratio, v/v) formed the mobile phase. The injection volume was 20 μL, with a flow temperature of 30°C and a flow rate of 1 mL/min. The amount of release was calculated and the cumulative release curve was plotted.

Mechanical strength and ex vivo skin insertion. Mechanical properties of MNPs were measured by a force test bench (TH-8203S, Tophung, China). Briefly, One MNP was placed in the center of the rigid stainless-steel platform (with the tips of the microneedle facing upward). The test station sensor probe moved toward the MNP at a speed of 0.1 mm/s. Force and displacement measurements began when the transducer first touched the microneedles tips and continued until the force applied to the transducer from the microneedles reached 70 N and stopped. After each test, the Microneedles were placed under a digital microscope (XTL-500, Jifei, China) to observe the change in shape of the microneedles.

Eight-layer parafilms were folded to achieve the thickness similarity to human skin for verifying the insertion capability of the prepared MNPs. Following attachment of the microneedles to the force sensors, the MNPs were vertically pressed into the parafilms with 10 N by force test bench. After separation, the layer was unfolded to evaluate the number of holes left in each layer and to further identify the detached MNPs embedded in the parafilm.

To verify the insertion capability of MNPs in skins, three simulated human skins (porcine skin, SD rat skin, 3% agarose hydrogel) were used. The dye-loaded MNPs were pressed onto the skins by thumb and held for 2 minutes. Subsequently, the MNPs were removed and the simulated skins were placed under chemiluminescence analyzer (4600SF, Tanon, China), CLSM and smart phone (iPhone 11, Apple, USA) to observe the pinholes.

Determination of the drug loading capacity of MNPs. The amounts of drug contained in the microneedles were calculated using the HPLC-UV method described previously. In brief, the microneedles of a MNP were scraped off by a blade and dissolved with 700 μL acetonitrile, then 300 μL water was added to fix the volume, shaken and filtered. HPLC-UV experimental conditions: reversed-phase C18 column (250 mm by 4.6 mm; inner diameter, 5 μm particle size). Acetonitrile and distilled water (7:3 ratio, v/v) formed the mobile phase. The injection volume was 20 μL, with a flow temperature of 30°C and a flow rate of 1 mL/min.

Rapid detachment of microneedles and base in vivo. MNP with R-B microneedles and C-6 base was applied to the shaved backs of adult female SD rats (200 g, Vital River, China) under chloral hydrate anesthesia by thumb and held for 1 minute. Subsequently, the green base of MNP was gently peeled from skin and the recovery of pinholes on the back of SD rats was observed.

Questionnaire survey on contraceptive preference. To investigate contraceptive preferences in different populations, 40 participants of different ages (20 to 60 years) and status (student, working, retired) were selected and asked a standard set of questions to solicit information about the acceptability of the biphasic contraceptive MNPs compared with other contraceptive methods.

Biocompatibility study of MNPs. On the second day after the application of the MNPs, blood samples were taken from each group of rats for serum biochemical analysis. At the end of the study, the rats were executed and the tissue around the patch application site was excised. The tissue was fixed in 10% neutral buffered formalin at 4°C for 48 hours, completely dehydrated and embedded in paraffin for sectioning and stained with H&E for histological analysis.

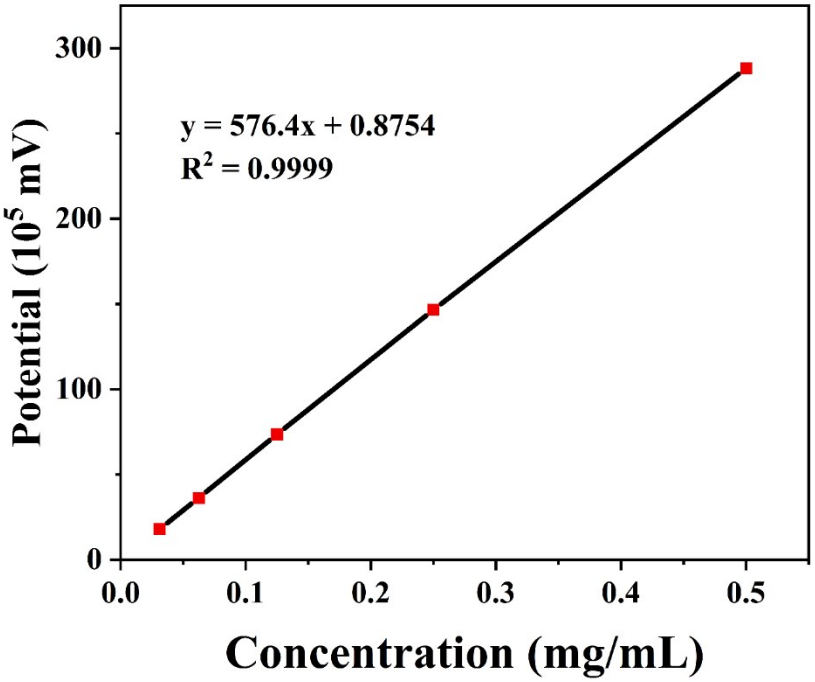

Figure S1. Linear correlation between peak area of HPLC-UV and LNG concentration. A linear plot of peak area versus LNG concentration was obtained with a correlation coefficient of 0.9999 in the detection range of 0.03125 mg/mL to 0.5 mg/mL.

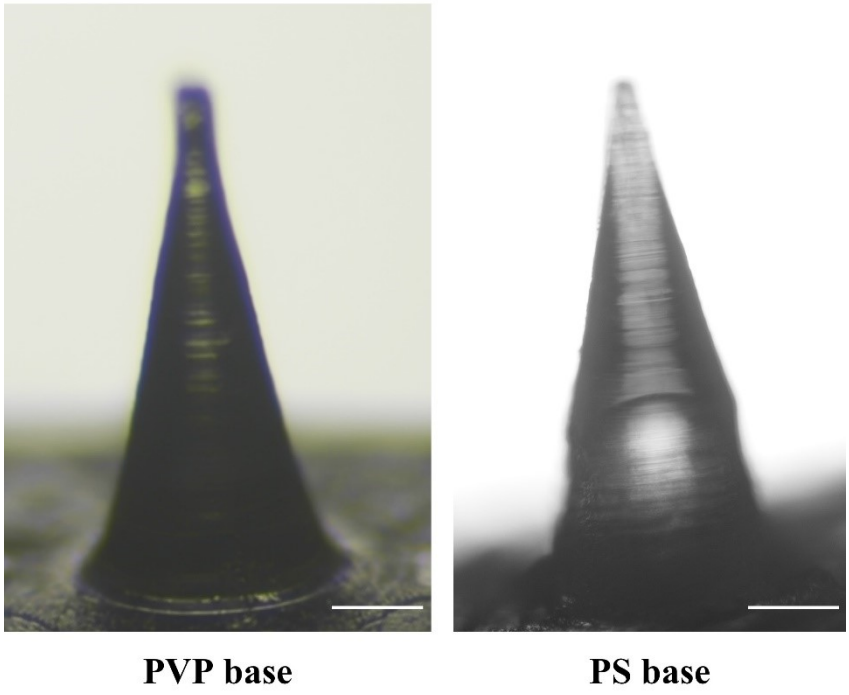

Figure S2. Bright microscope images of PVP-based and PS-based MNPs. Both of the two kinds of MNPs displayed similar conical morphology because they were produced from the same PDMS mold. Scale bars are 0.2 mm.

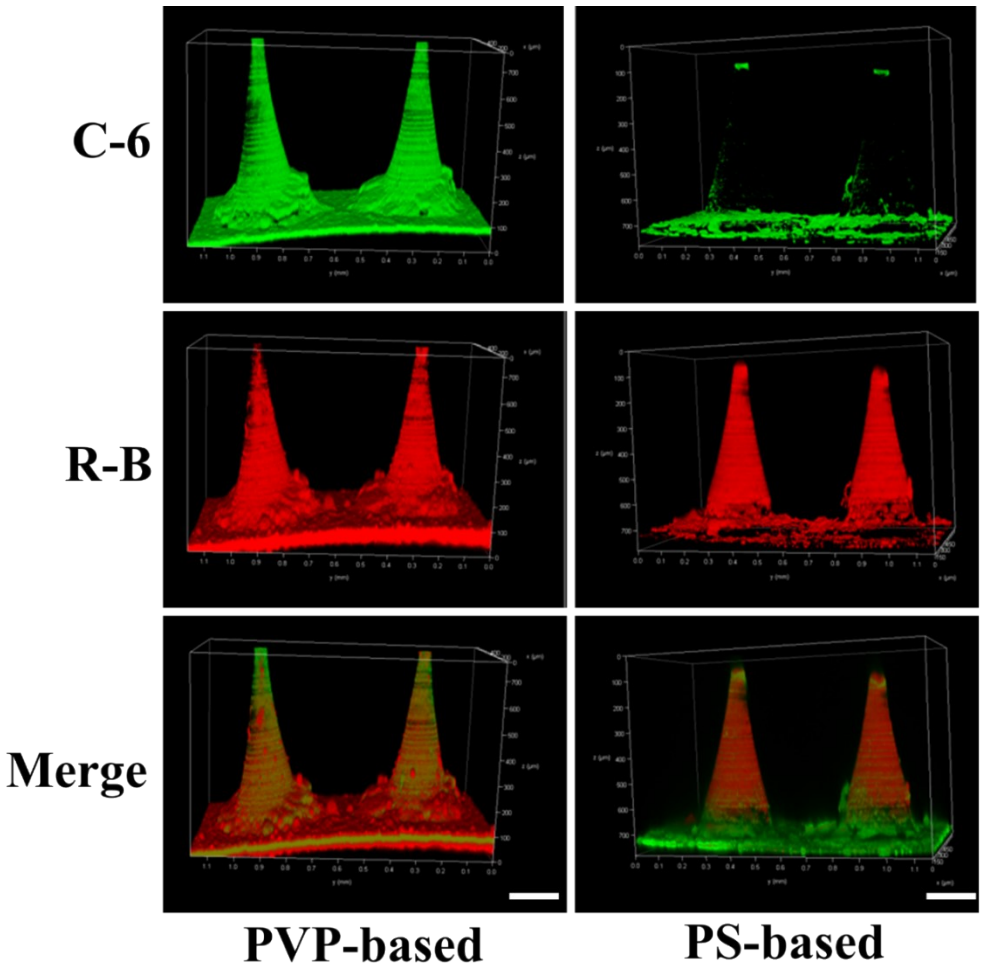

Figure S3. Confocal laser scanning microscopy images of MNPs using microneedles casting solution with R-B and base casting solution with C-6. Red and green were both loaded throughout the microneedles and base of PVP-based MNP, while for PS-based MNP, red only distributed in microneedles and green only displayed in base, which was attributed to the anti-diffusion effect of hydrophobic PS base. Scale bars are 0.1 mm.

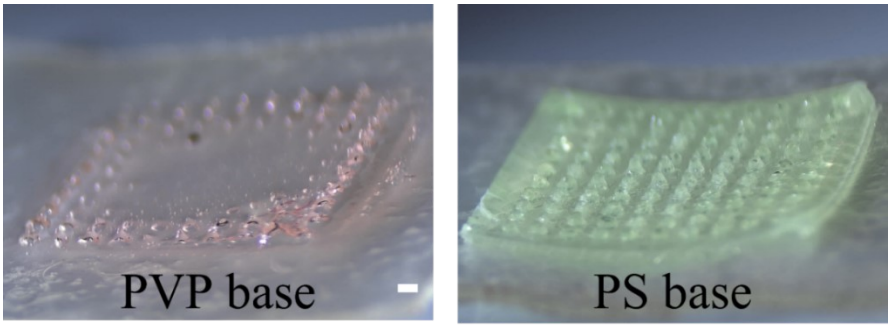

Figure S4. Comparative pictures of PVP-based and PS-based MNP solubility throughout the patch after insertion into porcine skin. Most of the centers of the PVP base have completely dissolved, while the PS base is intact and no red residue of microneedles was visible. Scale bars is 0.5 mm.

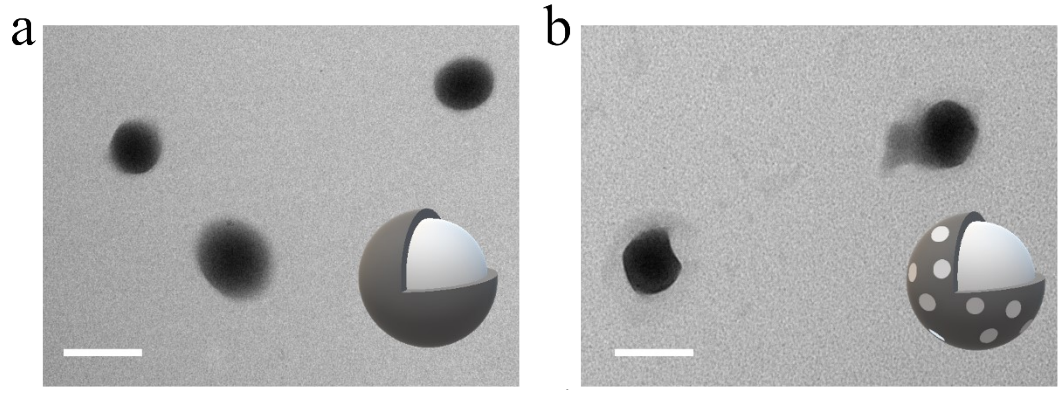

Figure S5. TEM images of multiple (a) LNG@PCL NCs and (b) LFP NCs. The inset pictures are schematic diagrams of the corresponding NCs. Scale bars are 200 nm.

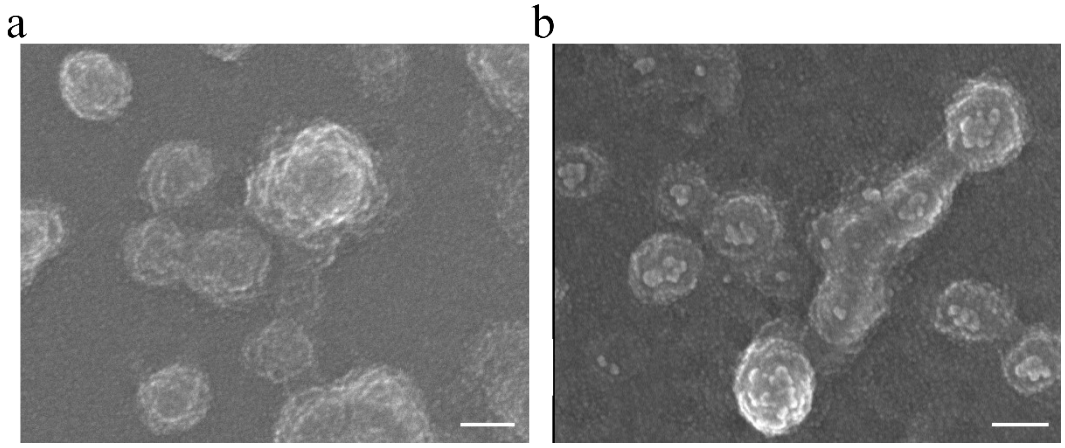

Figure S6. SEM images of (a) LNG@PCL NCs and (b) LPF NCs. Scale bars are 100 nm.

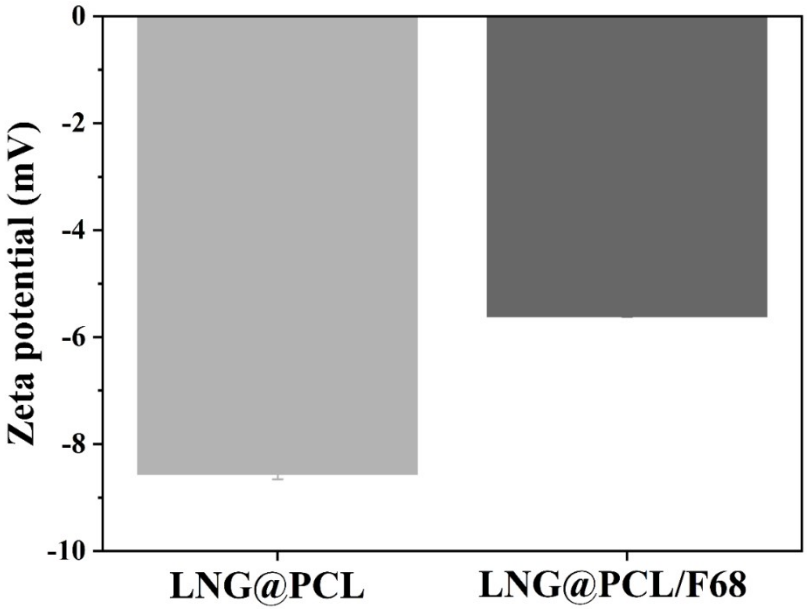

Figure S7. Zeta potential of LNG@PCL NCs and LNG@PCL/F68 (LPF) NCs. The LNG@PCL NCs was -8.565 ± 0.007 mV and LPF NCs was -5.615 ± 0.091 mV. All data are presented as mean ± SD (n = 3).

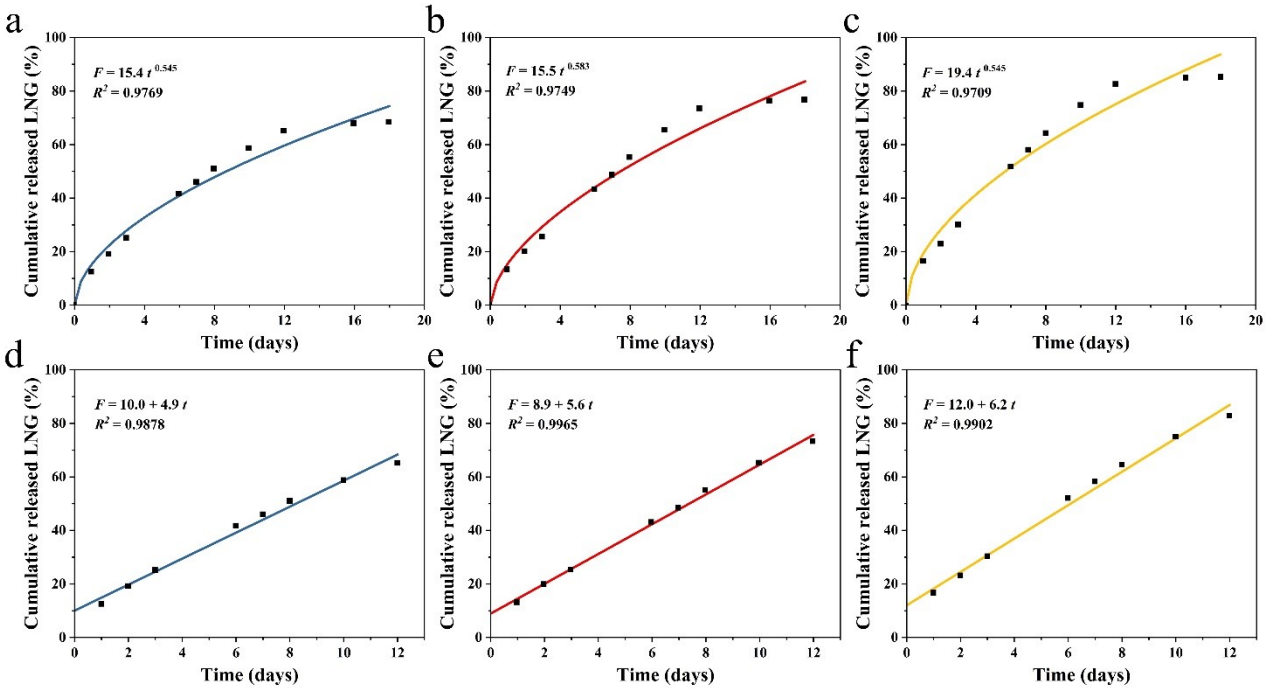

Figure S8. Fitted curves for kinetic models of LNG release from NCs with different F68 amounts. (a) Fitting curve of LNG from NCs with 0% F68 on Korsmeyer–Peppas model. (b) Fitting curve of LNG from NCs with 40% F68 on Korsmeyer–Peppas model. (c) Fitting curve of LNG from NCs with 60% F68 on Korsmeyer–Peppas model. (d) Fitting curve of LNG from NCs with 0% F68 on zero-order model. (e) Fitting curve of LNG from NCs with 40% F68 on zero-order model. (f) Fitting curve of LNG from NCs with 60% F68 on zero-order model.

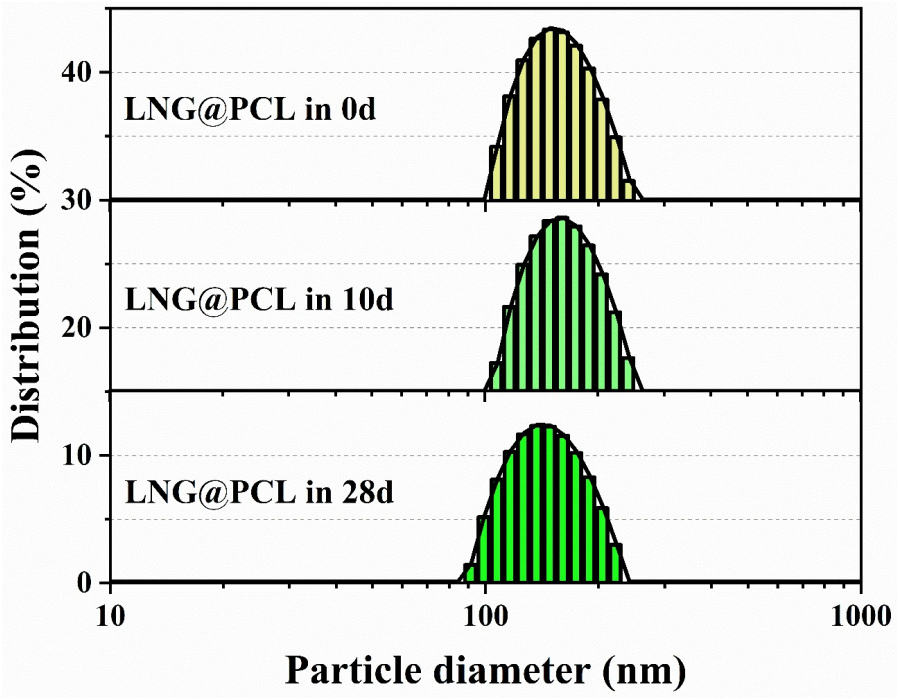

Figure S9. Dynamic light scattering of LNG@PCL NCs in three periods (0, 10 and 28 days). The particle sizes of LNG@PCL NCs were 160.26 nm (PDI = 0.19), 176.17 nm (PDI = 0.06) and 153.29 nm (PDI = 0.05), respectively. This indicated the excellent dispersibility and stability of LNG@PCL NCs.

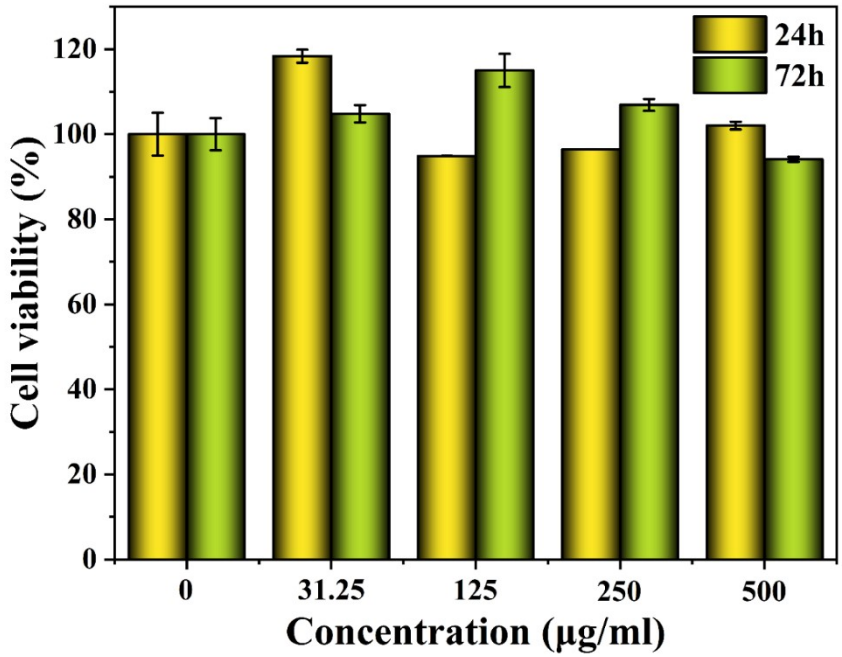

Figure S10. The survival rates of AGS cells after co-incubation with different concentrations of LPF NCs for 24 and 72 hours. The viability of AGS cells exceeded 90% up to 72 hours at any concentration, demonstrating the superior biocompatibility of LPF NCs. All data are presented as mean ± SD (n = 6).

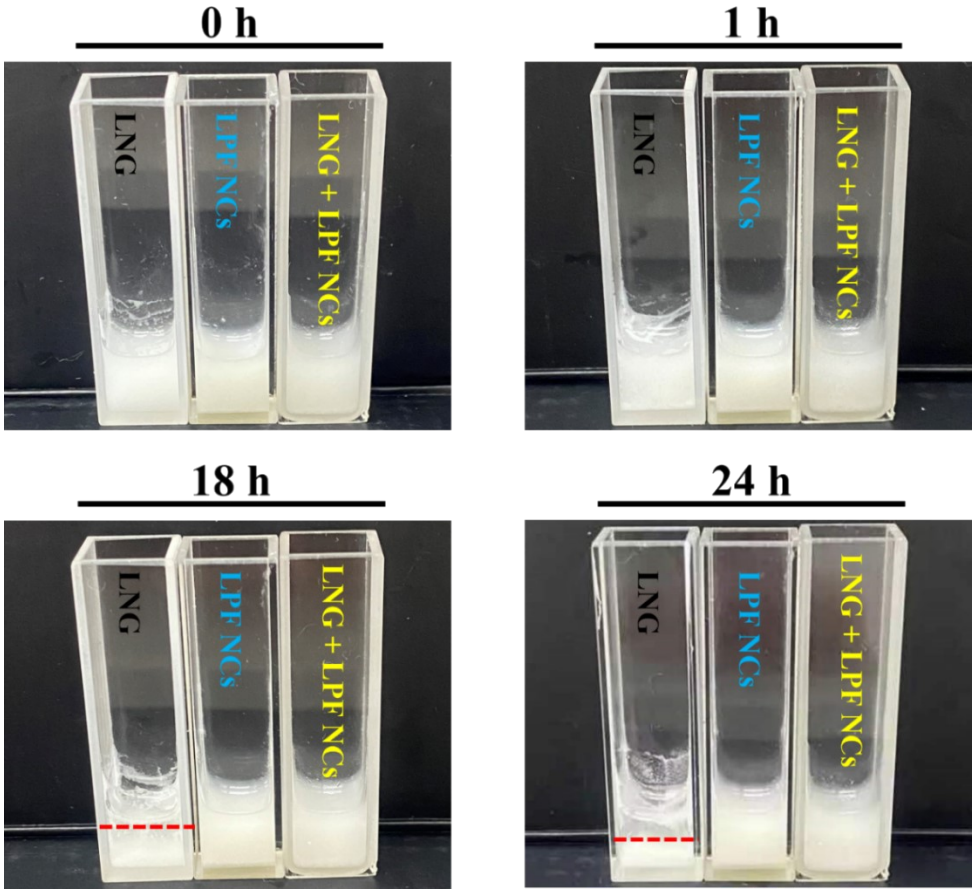

Figure S11. Uniform dispersion of LPF NCs within the matrix PVP. The red dashed lines indicate the layered interface. Pure LPF NCs and mixtures of LNG and LPF NCs could be kept in PVP at room temperature for more than 24 hours without sedimentation. In contrast, pure LNG had significant sedimentation because of strong hydrophobicity, and a delamination of the transparent PVP solution and the white LNG powders was observed. It was shown that the LNG-loaded NCs were well stabilized in PVP and this suspension had a positive effect on the consistency of the loading of the prepared MNPs.

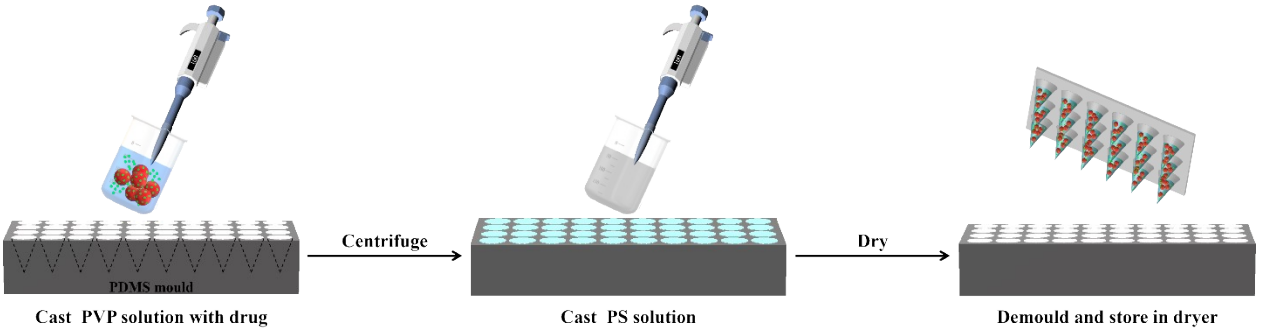

Figure S12. Preparation scheme of drug-loaded biphasic MNPs. LPF NCs MNPs and mixed MNPs (LNG and LPF NCs) were obtained by a previous two-step solution casting method, differing in the drug loading. For LPF NCs MNPs, the microneedles casting solution contained 40% (w/v) PVP loaded with pure LPF NCs with 10 mg LNG. For mixed MNPs, the microneedles casting solution contained 40% (w/v) PVP aqueous solution loaded with 5mg free LNG and LPF NCs with 5 mg LNG. Briefly, 50 μL of the prepared microneedle solution was applied by pipette to the PDMS mold to fill the microcavities. Then, 200 μL of base solution was casted and dried overnight at room temperature before demolding.

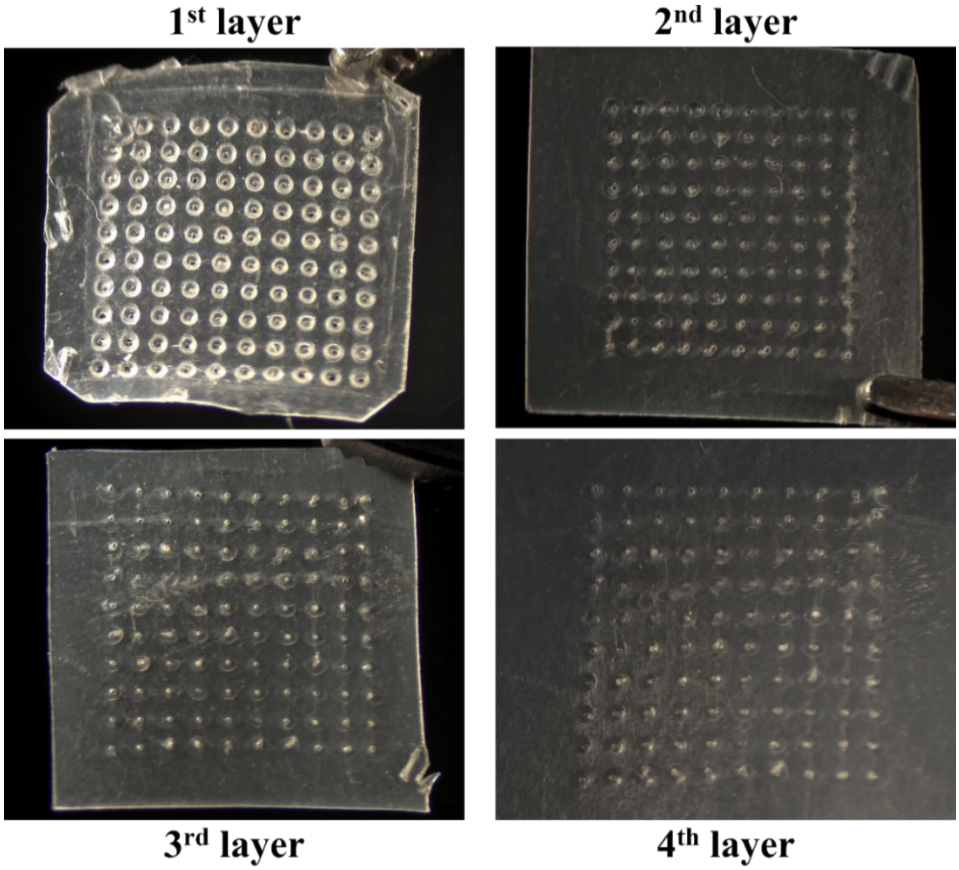

Figure S13. Pictures of the top four layers of parafilms after being punctured by MNPs. There were 100 clear pinholes in the first two layers, about 80 pinholes in the third layer, and over 50 pinholes in the fourth layer, demonstrating that 100% microneedles could penetrate the skin to a depth of 254 μm and more than half of the microneedles could reach 508 μm below the skin.

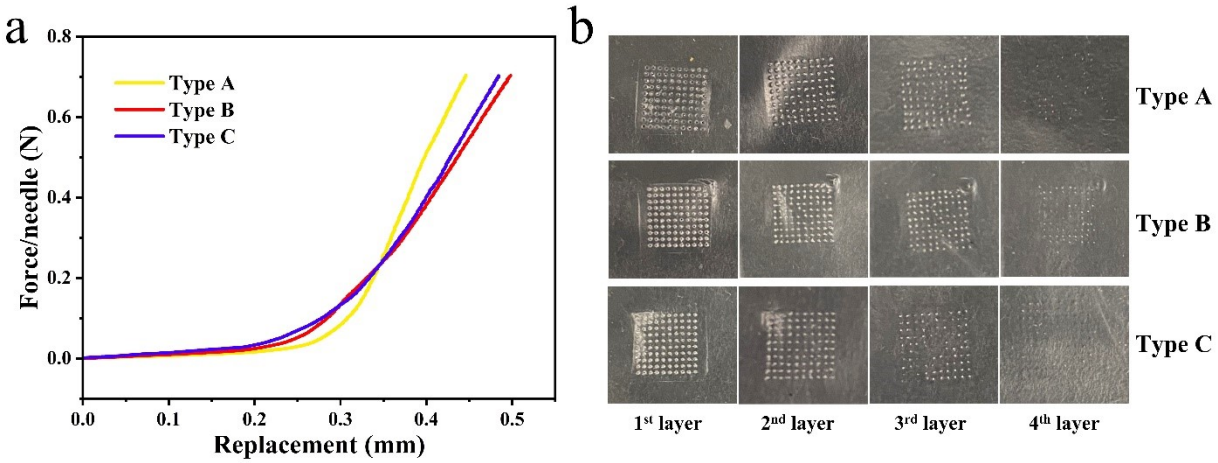

Figure S14. Mechanical properties and drug delivery abilities of the three types MNPs in vitro. (a) Schematic illustration of mechanical force of three types of MNPs by a force test bench. (b) Pictures of the top four layers of Parafilms after being punctured by three types of MNPs.

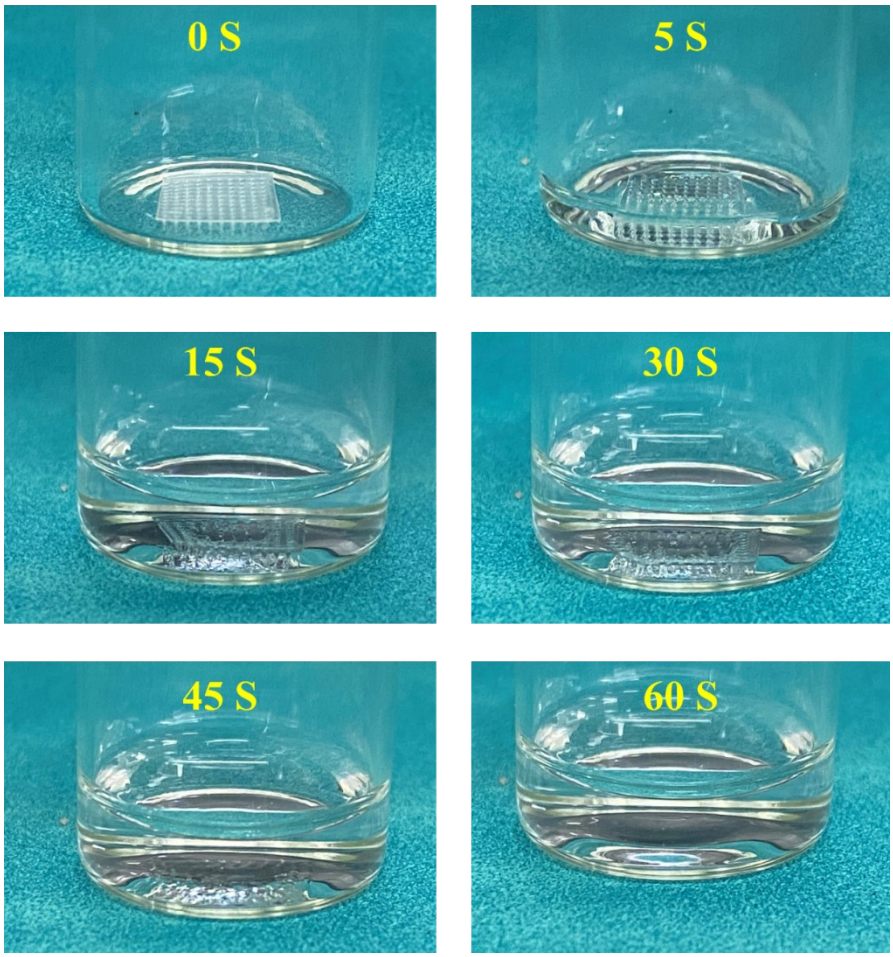

Figure S15. Solubility of drug-loaded MNP in PBS aqueous solution. This PVP microneedles dissolved rapidly within 60 seconds after the addition of PBS, indicating that the microneedles could dissolve quickly in skin and release LNG and LPF NCs.

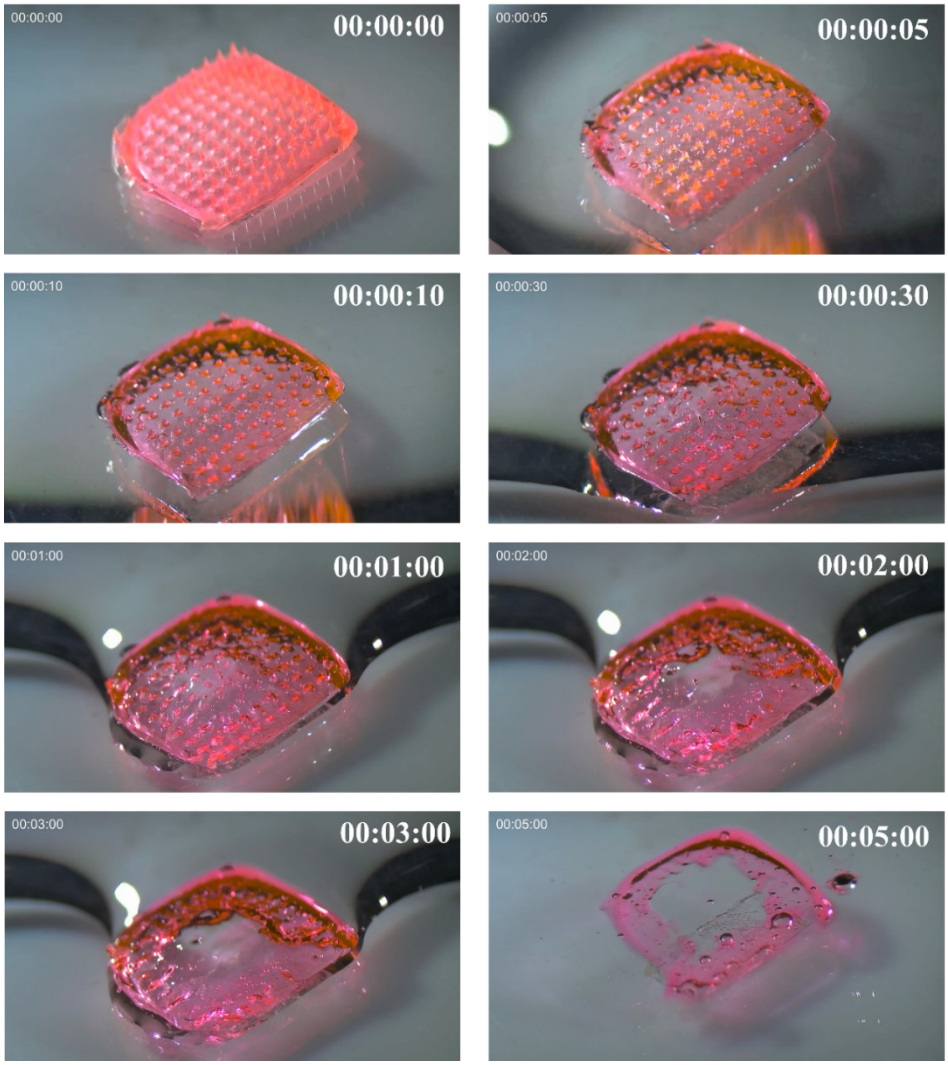

Figure S16. Solubility of PVP-based MNP with originally loading R-B and drug in microneedles and C-6 in base. Because of the rapid solubility of PVP, the red microneedles dissolved quickly when dropped into the PBS solution, accompanied by the dissolution of the PVP base.

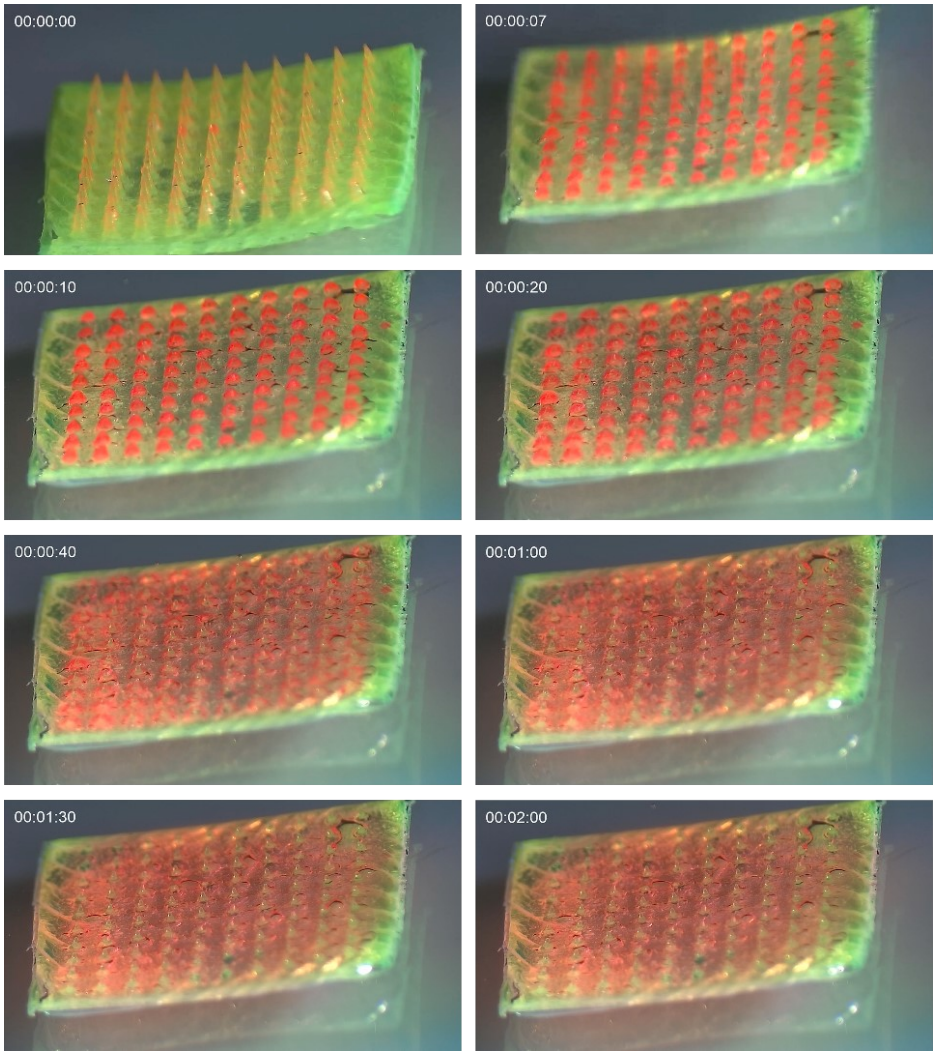

Figure S17. Solubility of PS-based MNP with originally loading R-B and drug in microneedles and C-6 in base. Because of the rapid solubility of PVP, the red microneedles dissolved quickly when dropped into the PBS solution, while the green PS base was able to maintain its intact form in PBS.

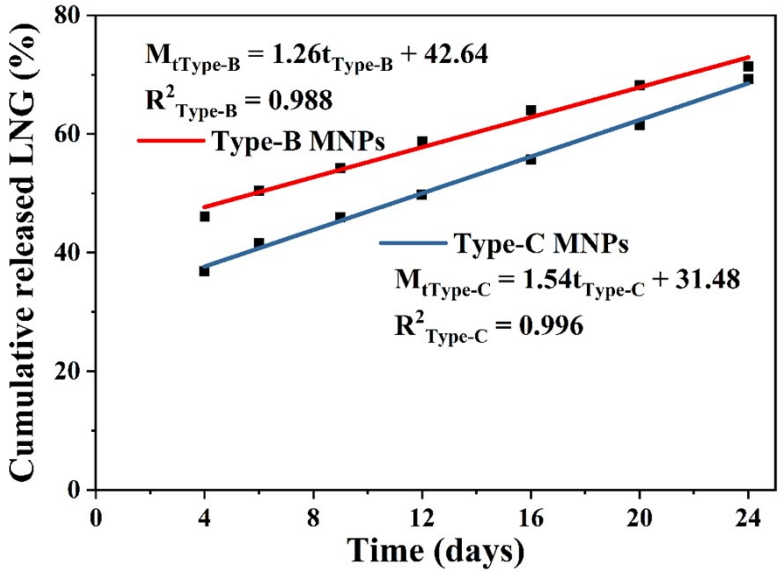

Figure S18. Zero-order release model of LNG controlled release formulation. The R^2 of Type-B and Type-C were 0.988 and 0.996 in zero-order model, demonstrated that the LNG release from NCs within MNPs was constant and continuous during the last 20 days.

Video S1. 3-D structure of dyes-loaded MNPs using soluble PVP base, imaged in z-stack mode of CLSM. Red: R-B. Green: C-6.

Video S2. 3-D structure of dyes-loaded MNPs using insoluble PS base, imaged in z-stack mode of CLSM. Red: R-B. Green: C-6.

Video S3. The microneedles dissolution of dyes-loaded MNPs with PVP base. The red PVP microneedles dissolved immediately after the addition of PBS, accompanied by the dissolution of the mixture of red and green PVP base. The entire MNP was completely dissolved within 5 minutes. Red: R-B. Green: C-6.

Video S4. The microneedles dissolution of dyes-loaded MNPs with PS base. The red PVP microneedles of PS-based MNP were dissolved immediately after the addition of PBS, which was consistent with PVP-based MNPs. Whereas, the green PS base layer showed no sign of dissolution in PBS. Red: R-B. Green: C-6.

Video S5. The rapid separation of R-B microneedles and C-6 base of the biphasic MNPs in rat. The dye MNP was administered in SD rat and left on the skin for 1 min, then the green PS base was gently peeled off the skin with forceps.